Title

Optical coherence tomography and Raman spectroscopy of the retina

ISBN

9780819474179

Authors

Evans, Julia W

Zawadzki, Robert J

Liu, Rui

et al.

Publication Date

2009-02-12

DOI

10.1117/12.807885

Peer reviewed

Optical coherence tomography and Raman spectroscopy of the retina

Julia W. Evans[a,b,c], Robert J. Zawadzki[b], Rui Liu[c], James W. Chan[a,c], Stephen M. Lane[c], John S. Werner[b]

[a]Lawrence Livermore National Laboratory
7000 East Avenue, Livermore 94550

[b]Vision Science and Advanced Retinal Imaging Laboratory, Department of Ophthalmology & Vision Science, University of California, Davis,
Sacramento, CA 95817

[c] NSF Center for Biophotonics Science and Technology, University of California, Davis,
Sacramento, CA 95817

ABSTRACT

Imaging the structure and correlating it with the biochemical content of the retina holds promise for fundamental research and for clinical applications. Optical coherence tomography (OCT) is commonly used to image the 3D structure of the retina and while the added functionality of biochemical analysis afforded by Raman scattering could provide critical molecular signatures for clinicians and researchers, there are many technical challenges to combining these imaging modalities. We present an *ex vivo* OCT microscope combined with Raman spectroscopy capable of collecting morphological and molecular information about a sample simultaneously. The combined instrument will be used to investigate remaining technical challenges to combine these imaging modalities, such as the laser power levels needed to achieve a Raman signal above the noise level without damaging the sample.

Keywords: Raman Spectroscopy, Optical Coherence Tomography, Retinal Imaging

1. INTRODUCTION

Optical coherence tomography is a powerful volumetric imaging modality that has proven to be successful for *in vivo* imaging of the retina. It is commonly used by clinicians and researchers both to diagnose and monitor eye diseases and for improving our understanding of the structure of healthy eyes. Often functional tests (e.g., visual fields) can be correlated with changing structures in the eye, which are imaged with OCT, for a more complete understanding of eye function and disease. Raman spectroscopy is a spectroscopic method based on inelastic (also known as Raman) scattering that allows the biochemical composition of a sample to be identified. The combination of OCT and Raman spectroscopy could provide new insights into the retina. Here we describe a combined instrument for *ex vivo* measurement of the retina.

OCT is an imaging modality that allows high volumetric resolution (few μm) mapping of the scattering intensity from the sample. OCT is similar to ultrasound techniques, but the intensity of back-scattered light rather than sound waves is measured as a function of depth (in the tissue). Due to the fast speed of light, direct measurements of the time of flight, as in ultrasound, are not possible. Instead a low-coherence light source (or swept laser) and an interferometer with a sample arm and a mirror in the reference arm have to be implemented to reconstruct the depth position of each back-scattered photon. OCT in the time domain has become an essential tool in the diagnosis and treatment monitoring of human retinal disease.[1] In this method the position of the reference mirror varies allowing the axial shift of the coherence gate (zero path length difference position in the sample). Because of the coherent detection scheme only photons from within the coherence gate can be detected. Thus, by applying constant speed to the reference mirror a back-scattering intensity profile from the sample can be recorded as a function of time. Fourier-domain OCT (FD-OCT)[2–4] is an alternative to time-domain OCT where no scanning reference mirror is necessary and the whole depth scattering profile can

Send correspondence to evans74@llnl.gov

Multimodal Biomedical Imaging IV, edited by Fred S. Azar, Xavier Intes, Proc. of SPIE Vol. 7171, 71710O · © 2009 SPIE · CCC code: 1605-7422/09/$18 · doi: 10.1117/12.807885

be reconstructed by Fourier transformation of spectral fringes recorded by a spectrometer for a single reference mirror position. This parallel detection (whole depth profile is measured from one spectral fringe) offers a significant advantage in sensitivity and acquisition speed over the standard time-domain OCT technique. The high speed of Fourier-domain OCT permits the 3D imaging of *in vivo* retinal structures. More recent attempts to acquire functional data (beyond scalar scattering profiles) have also been demonstrated with Doppler FD-OCT (flow measurements),[5] polarization-sensitive FD-OCT (birefringence measurements)[6] as well as multi-functional systems.[7] Development of OCT systems for ophthalmic applications including adaptive optics OCT are a major thrust of the research in the Vision Science and Advanced Retinal Imaging Laboratory at UC Davis.[8]

The Raman scattering process, which was first discovered by C.V. Raman in 1928, involves the inelastic scattering of photons by molecular bonds.[9] When a material is illuminated by monochromatic light at an arbitrary wavelength, a small fraction of the photons will be scattered with a frequency shift that is directly related to the vibrational or rotational states of the molecular bonds in the material. Therefore, Raman spectroscopy is a powerful optical method for molecular detection and characterization that is applicable to a wide variety of disciplines (e.g., physics, biology, chemistry, and material science). In biology and biomedicine, Raman spectroscopy is particularly attractive because it provides molecular level information without the need to use exogenous fluorescent labels or to perturb the sample using stains or chemical fixatives, and offers potential for *in vivo* interrogation. The unique molecular signatures provided by a Raman spectrum allow biologists and clinicians to gain insight into disease progression at both the tissue and cellular levels.[10]

The application of Raman spectroscopy in ophthalmology offers the potential for acquiring real-time, *in vivo* chemical and functional information not easily obtained by other interrogation methods.[11] However, implementing Raman spectroscopy for *in vivo* detection is challenging, because of the high laser-excitation intensities required to obtain a sufficient signal-to-noise ratio spectrum, which can easily damage delicate eye tissues. While resonance Raman spectroscopy can be used to circumvent this issue by allowing for the use of low exposure conditions,[12] it only provides for the detection of specific resonant molecules. For a broader characterization of the entire molecular composition of the tissue (e.g., proteins, fatty acid based lipids, DNA, saccharides, cytochromes/hemes), spontaneous Raman spectroscopy is a more suitable method, but encounters the potential damage issues mentioned above. The advances in sophisticated optical design in conjunction with sensors with high quantum detection efficiency make *ex vivo* or even *in vivo* applications of Raman spectroscopy potentially feasible. Previously, Beattie et al have systematically studied the retina *ex vivo* with confocal Raman microscopy under different excitation wavelengths and obtained significantly different Raman spectrum from different layers of retina, which shows the potential of Raman spectroscopy as a clinical diagnostic tool for retina and related neurological diseases.[13]

In this paper, we report on the preliminary development and characterization of a Raman spectroscopy system in combination with OCT to obtain simultaneous chemical and structural information. This system will be used to characterize, *ex vivo*, the minimum power densities required to obtain Raman spectra of retinal tissue to determine the feasibility of *in vivo* retinal Raman/OCT characterization. A similar instrument for OCT guided Raman was built by Patil et al.[14] In the Patil et al instrument, individual Raman spectrum are collected based on the previous completed OCT volume. Their instrument is also designed for skin tissues and has correspondingly higher power levels. In comparison, our instrument will focus on retinal tissue and allows for the simultaneous acquisition of Raman and OCT signals. Collecting Raman spectrum at each OCT location introduces challenges to the instrument, but also allows a mapping of the Raman signature of different molecules to be correlated to the structure of the sample as measured by OCT. We present data collected from a non-biological sample and an *ex vivo* human retina used to demonstrate that the instrument is functional.

2. DESCRIPTION OF INSTRUMENT

As with many standard OCT systems we used a Michelson interferometer configuration with a reference and a sample arm. Both are shown in Fig.1. The sample arm is effectively a confocal microscope with OCT detection allowing reconstruction of back-scattering intensity depth profiles within the depth of field of the confocal beam. The initial focus position is adjusted by axially shifting the whole sample arm using an attached micrometer. Lateral scanning is achieved by an automated x-y translation stage on which the sample is placed. OCT axial resolution depends on the light source used for imaging and in our case was on the order of 4.5 μm ($\lambda_0 = 855$ nm;

$\Delta\lambda = 75$ nm). Lateral resolution (similar to standard confocal microscopy) is set by the imaging optics and is about 18 μm. OCT single line exposure time is usually set to 50 μm. Typically 8 linescans are averaged for each position in the sample. During scanning the Raman subsystem requires a significantly longer exposure time and the exposure times noted in the rest of the section refer to the Raman exposure, while the OCT exposure time remains the same. To the original OCT sample arm a separate excitation and collection channel has been added

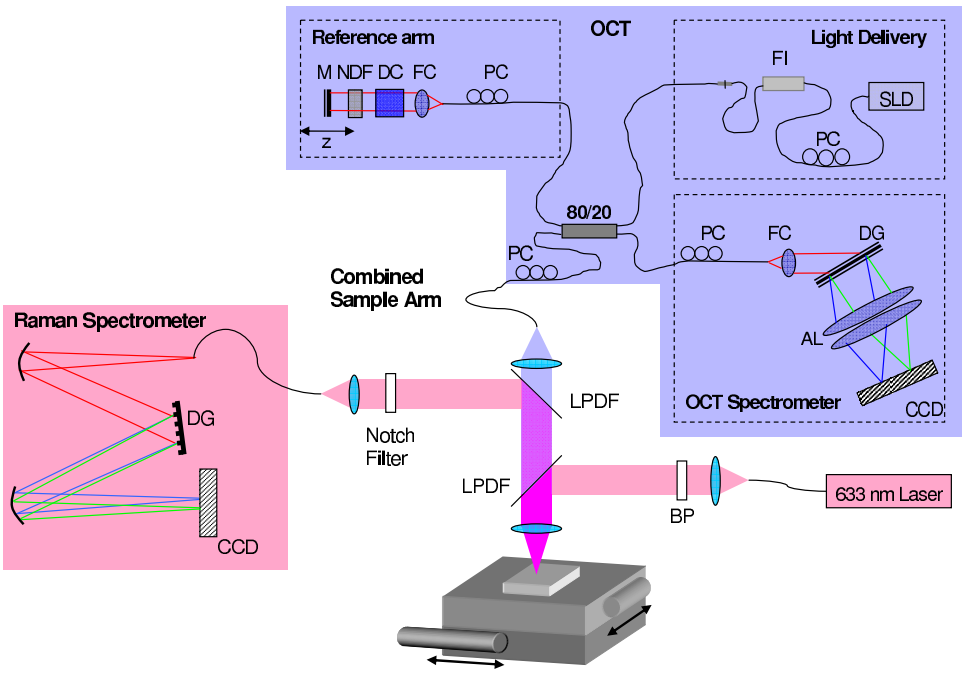

Figure 1. Layout of the combined OCT and Raman spectrometer. M: Mirror, NDF: Neutral Density Filter, DC: Dispersion Compensation, FC: Fiber Coupler, PC: Polarization Control, FI: Fiber Isolator, SLD: Super Luminescent Diode, DG: Diffraction Grating, AL: Achromatic Lens, BS: Beam splitter, LPDF: Long Pass Dichroic Filter, BP: Bandpass Filter

for a Raman spectrometer. The combined system (including both OCT and Raman detection spectrometers) is on a 3 foot by 2 foot optical table that can be wheeled through doorways for some portability. Figure 2 is a photograph of the combined system.

The Raman spectrometer subsystem has a fiber optic confocal configuration to reduce stray background light. The excitation light source of the system is a single-mode fiber coupled to a 632.8 nm He-Ne laser. This is collimated by an objective and the laser line of the collimated beam is cleaned up by a narrow band-pass filter to remove the plasma lines from the He-Ne laser. The cleaned up laser beam is then reflected by a long pass dichroic filter (LPDF) and finally focused on the sample through an achromat. In the current set up approximately 4 mW of He-Ne laser light are delivered to the sample. This is in contrast to other Raman systems. For example, Patil et al[14] deliver 40 mW to the sample. We chose a lower light level to correspond more closely to the conditions needed for *in vivo* retinal imaging. The emitted Raman signal is collected by the same achromat and transmitted through the first LPDF and is reflected by a second LPDF. The reflected Raman signal passes through a notch filter to remove the Rayleigh scattering from the sample and finally focuses to a multi-mode fiber coupled spectrometer. The multi-mode fiber has a 50 μm core and serves as the pinhole in the confocal system to reject the out-of-focus background light. The spectral resolution of our confocal micro-Raman setup is estimated to be approximately 5 cm^{-1}.

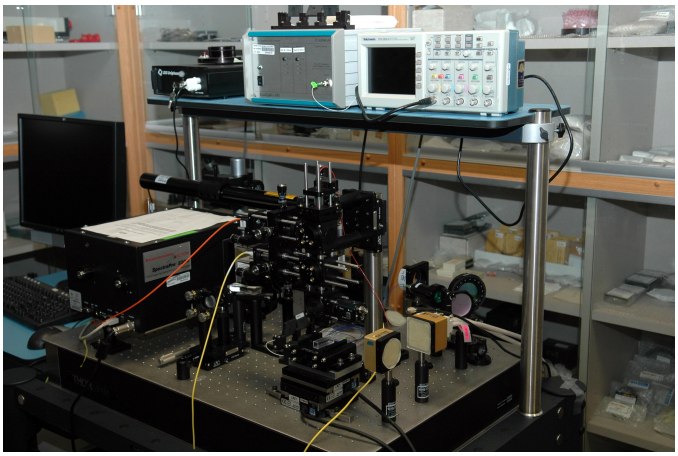

Figure 2. Picture of combined OCT-Raman system

The combined OCT-Raman microscope was primarily built from parts on hand and aspects of its operation could be improved through improved design. In particular, the throughput of light from the sample could be optimized with slightly different optical components.

3. RESULTS AND DISCUSSION

The combined OCT-Raman instrument collects an OCT and Raman signal from each point on a grid over the sample. Each OCT sample is a depth scan (A-scan) and each Raman signal is one spectrum. Both sets of data presented here were measured over a 4 mm square with 400 samples in one axis and 80 in the other. The size and sampling of the scan are limited by how long the data acquisition takes. Both of these scans took several hours and the samples would dry out if longer experiments were performed. The OCT data are processed and rendered into a volume in the same way that *in vivo* data are processed. This method is described in previous works including Zawadzki et al.[8] The data can be viewed as a volume (See Fig. 6) or in cross section (See Fig. 5). A Raman spectrum is collected for each A-scan but because of poor signal to noise the spectra are generally averaged over neighboring samples. The spectrum have a polynomial fit subtracted to remove florescence following the technique of Vickers et al.[15] The intensity of the spectrum has not been calibrated to correspond to the amount of any particular substance in the sample so the spectrum are shown with an arbitrary scale.

3.1 Non-Biological Phantom

For testing the combined Raman-OCT system a non-biological phantom was constructed of two samples (polystyrene and a second polymer sample) imbedded into a stable gel matrix. The goal of this test was to demonstrate that two structures that could not be distinguished by OCT alone could be distinguished by the combined instrument. The spectrum of the two samples was measured first in Raman only mode with a 5-second exposure and the spectra are compared in Fig. 3. The signal from the second polymer sample is dominated by florescence, which has been removed by the polynomial fit, and the remaining spectrum is weaker than the polystyrene signal. In this case the intensity of the signal is divided by the standard deviation of a region of the spectrum with no peaks (a pseudo signal-to-noise ratio). A shorter integration time is necessary in scanning mode of the instrument to avoid an overly long integration time during which the sample can dry out. An OCT volume and corresponding Raman Map were acquired for the sample with a 200 ms integration time. An average spectrum from the polystyrene sample collected during combined OCT and Raman acquisition is compared to the signal obtained with the 5-second integration time from the sample alone in Fig. 4. The Raman signal from the second polymer sample is not visible with the short (200 ms) integration time. As described above, the signals are divided by the standard deviation of a region in the spectrum with no peak. Capturing individual Raman spectrum from the sample with a longer integration time does yield higher signal to noise, but the advantage of acquiring a Raman Spectrum at each A-Scan of the OCT data is the ability to generate Raman maps which

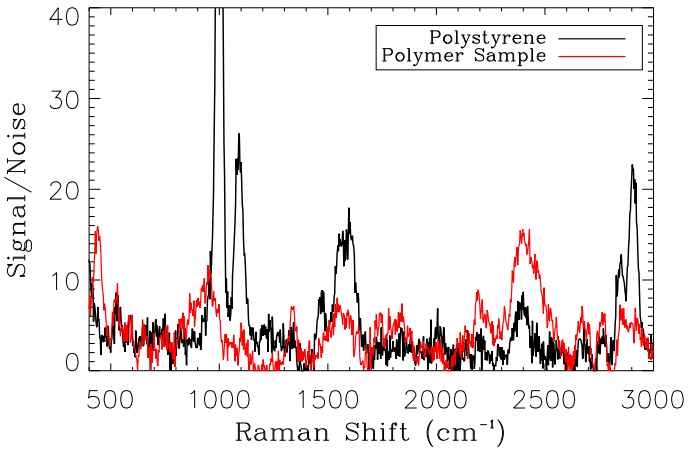

Figure 3. Comparison of Raman spectra from the polystyrene and second polymer sample when not imbedded in the gel sample. The integration time for these samples was 5 seconds, much longer than the integration time during combined OCT-Raman acquisition. The two polymers have different Raman signals. Signals are divided by the standard deviation of a region in the spectrum with no peak and a polynomial fit is removed.

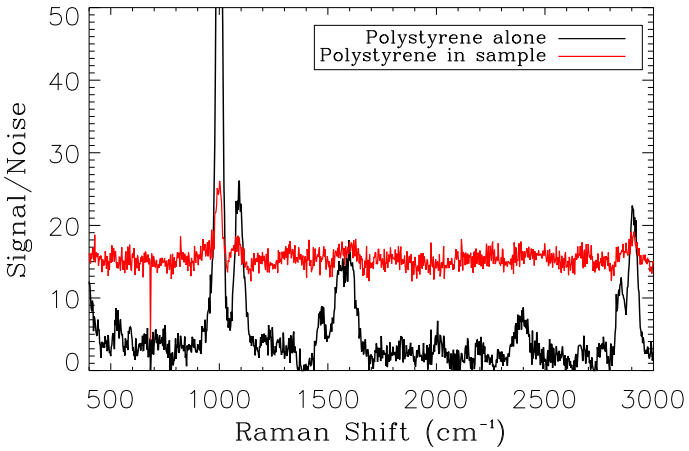

Figure 4. Comparison of Raman Spectra from the polystyrene collected with the long integration time and from an average over 10 x 10 samples collected during combined Raman and OCT acquisitions. The Raman signal of the second polymer sample is not visible with the short (200 ms) integration time. Signals are divided by the standard deviation of a region in the spectrum with no peak. While the signal-to-noise ratio is clearly smaller (and the background comprises more of the signal), characteristic peaks identified in the longer integration time are still visible.

correspond to OCT volumes. Figure 5 shows such a comparison. The image on the left (a) is a cross section from the OCT volume. This sample was not ideal for OCT as it is relatively transparent, but the basic structure of the phantom and the placement of the two crystals are quite visible (there are also some air bubbles in the sample and few artifacts from multiple reflections). A Raman map can be generated showing the signal for a particular Raman shift for each location in the sample. These spectra are processed in the same way that the individual spectra shown above are (i.e., the polynomial fit is removed before the map is generated). The Raman map in Fig. 5 corresponds to the peak of the polystyrene at about 1000 cm^{-1}. To make the crystal more visible the map is divided by the average map from a region in the spectrum with no peaks. The other sample is not visible in any of the frames.

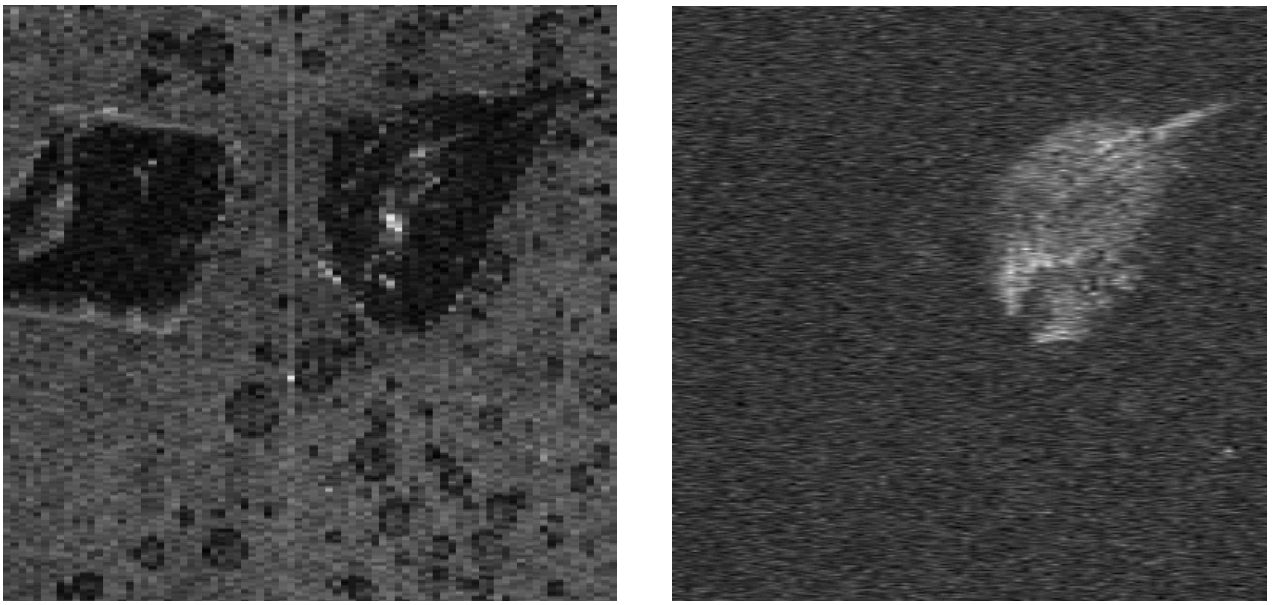

Figure 5. OCT reconstructed C-scan compared to Raman Map at polystyrene peak. In the OCT image both samples are visible, but in the Raman Map the polystyrene is clearly distinguished from the other polymer sample. The Raman map is averaged over 10 frames centered at the brightest peak of the polystyrene (1000 cm^{-1}).

3.2 Retina Sample

An *ex vivo* retina sample was also imaged with the combined OCT-Raman system. This sample is not fresh, but has been preserved in glutaraldehyde for several months. Scanning through the Raman maps at different Raman shifts there appears to be a variation in signal at the fovea compared to other areas of the retina. One such frame is shown with the corresponding OCT volume in Fig. 6. Unlike the phantom from the previous section this map is not divided by the background of the image, as it was difficult to find a region of the spectrum that was only background. Examination of the averaged spectrum over individual regions of the Raman map reveals a difference in the intensity of the signal, but there does not appear to be a change in the components that make up the spectrum from each region. Figure 7 is the averaged spectrum over the three regions indicated in Fig. 6. The shape of these three spectra appears to be the same, and if they are normalized by the average intensity of each spectrum they appear almost identical. We suspect the lack of variation between structures in the retina, which has been observed by others,[13] is caused by degradation in the sample. Comparison to other retina data also seems to indicate that we have additional Raman peaks probably introduced by the preservative and not from the retina itself. We do note that a Raman signal is measurable from the sample even with the short (200 ms) integration time. Signal-to-noise calculations are uninteresting without a specific Raman peak to examine. In fresher samples the variation in Raman spectrum between structures should be more obvious, particularly without the extra signal from the preservative. It is also possible that our low signal-to-noise will prevent us from seeing the Raman signal from some structures in the eye. Variation between healthy and diseased samples would also be interesting.

4. CONCLUSIONS AND FUTURE WORK

We have demonstrated a combined OCT-Raman microscope capable of collecting OCT volumetric data and biochemical Raman spectral maps simultaneously. As has been observed by other groups[14] the addition of Raman Spectrometry to OCT allows similar physical structures in the sample to be distinguished based on their chemical composition. We have collected an initial data set using an *ex vivo* human retina to demonstrate the functionality of the instrument. Challenges to improved data collection include the weakness of the Raman signal

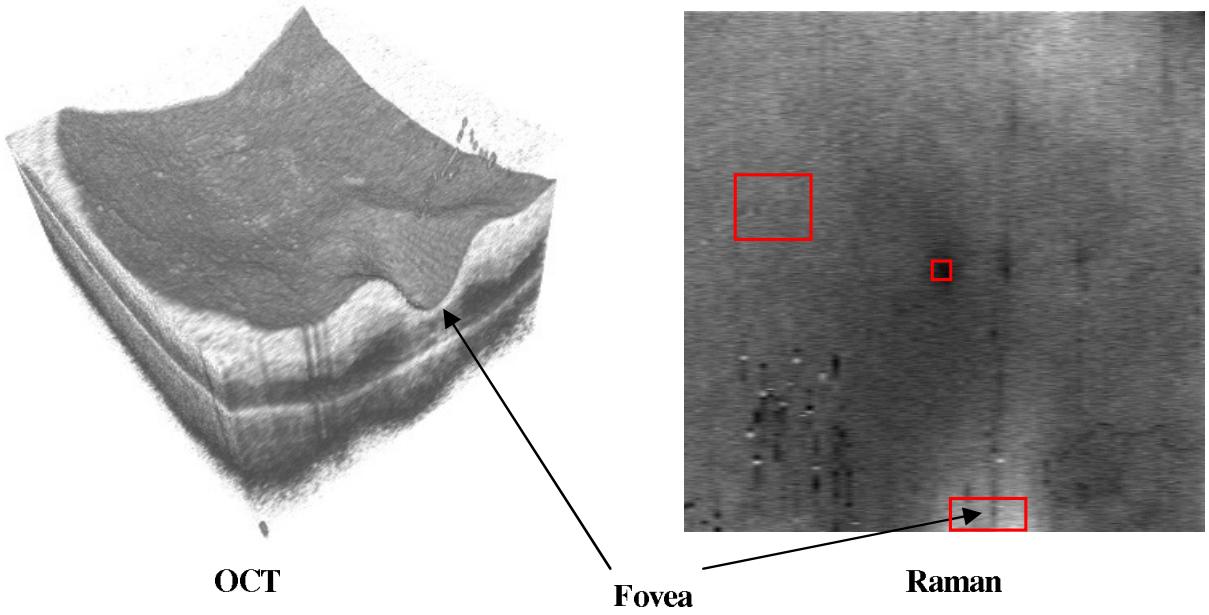

Figure 6. OCT volume from retina sample compared to raman map. The signal is clearly stronger in the region of the fovea.The Raman map is the average over wavenumbers 2369 to 2454 cm^{-1}. These frames were picked out for the brightness of the fovea not based on a specific biochemical marker. The red boxes indicate regions the Raman spectrum are averaged over for Fig. 7.

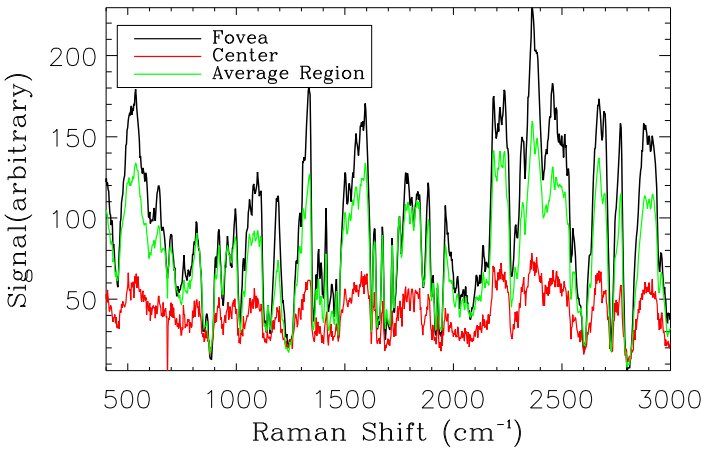

Figure 7. Raman spectrum averaged over the three regions indicated in Fig.6. The variation in intensity seen in the Raman Map is also clear in the spectra. These are not normalized to background, but when normalized to the average intensity the differences between the three regions are not present indicating that the Raman map shows a difference in intensity of Raman signal, but not a difference in the peaks of the spectra.

and difficulty of obtaining good samples for testing. Longer integration times would improve signal to noise, but would require a method of sustaining the sample over the long acquisition process. Optical components could be optomized to improve the efficiency of light delivery and collection, but this will most likely yield only a small improvement over the current system. Wavelength selection for the Raman and OCT systems, such as using longer wavelength Raman excitation light (e.g. 785 nm), or more advanced time gating methods to separate the Raman signal from the autofluorescence can also be investigated to improve the signal from the retina

samples. The next steps in this project are to acquire data for more samples. Animal model and human retina samples should be imaged and if obtainable a comparison of diseased and healthy retinas would be interesting. Investigation of these samples could provide interesting information about the biochemical make up of the retina and how it varies across samples and subjects, while also informing the design of a possible *in vivo* system.

4.1 ACKNOWLEDGMENTS

This research was supported by the National Eye Institute (grant EY 014743). This work was supported by funding from the National Science Foundation. The Center for Biophotonics, an NSF Science and Technology Center, is managed by the University of California, Davis, under Cooperative Agreement No. PHY 0120999. This work performed under the auspices of the U.S. Department of Energy by Lawrence Livermore National Laboratory under Contract DE-AC52-07NA27344.

REFERENCES

1. D. Huang, E. Swanson, C. Lin, J. Schuman, W. Stinson, W. Chang, M. Hee, T. Flotte, K. Gregory, C. Puliafito, *et al.*, "Optical coherence tomography," *Science* **254**(5035), pp. 1178–1181, 1991.
2. A. Fercher, C. Hitzenberger, G. Kamp, and S. El-Zaiat, "Measurement of intraocular distances by backscattering spectral interferometry," *Optics Communications* **117**(1-2), pp. 43–48, 1995.
3. M. Wojtkowski, R. Leitgeb, A. Kowalczyk, T. Bajraszewski, and A. Fercher, "In vivo human retinal imaging by Fourier domain optical coherence tomography," *Journal of Biomedical Optics* **7**, p. 457, 2002.
4. N. Nassif, B. Cense, B. Park, M. Pierce, S. Yun, B. Bouma, G. Tearney, T. Chen, and J. de Boer, "In vivo high-resolution video-rate spectral-domain optical coherence tomography of the human retina and optic nerve," *Optics Express* **12**(3), pp. 367–376, 2004.
5. R. Leitgeb, L. Schmetterer, W. Drexler, A. Fercher, R. Zawadzki, and T. Bajraszewski, "Real-time assessment of retinal blood flow with ultrafast acquisition by color Doppler Fourier domain optical coherence tomography," *Optics Express* **11**(23), pp. 3116–3121, 2003.
6. Y. Yasuno, S. Makita, Y. Sutoh, M. Itoh, and T. Yatagai, "Birefringence imaging of human skin by polarization-sensitive spectral interferometric optical coherence tomography," *Optics Letters* **27**(20), pp. 1803–1805, 2002.
7. B. Park, M. Pierce, B. Cense, S. Yun, M. Mujat, G. Tearney, B. Bouma, and J. de Boer, "Real-time fiber-based multi-functional spectral-domain optical coherence tomography at 1.3 μm," *Optics Express* **13**(11), pp. 3931–3944, 2005.
8. R. Zawadzki, S. Choi, S. Jones, S. Oliver, and J. Werner, "Adaptive optics-optical coherence tomography: optimizing visualization of microscopic retinal structures in three dimensions," *Journal of the Optical Society of America A* **24**(5), pp. 1373–1383, 2007.
9. C. Raman And K. Krishnan, "A new type of secondary radiation," *Nature* **121**(3048), p. 501, 1928.
10. E. Hanlon, R. Manoharan, T. Koo, K. Shafer, J. Motz, M. Fitzmaurice, J. Kramer, I. Itzkan, R. Dasari, and M. Feld, "Prospects for in vivo Raman spectroscopy," *Physics In Medicine And Biology* **45**(2), pp. 1–1, 2000.
11. R. Erckens, F. Jongsma, J. Wicksted, F. Hendrikse, W. March, and M. Motamedi, "Raman Spectroscopy in ophthalmology: From experimental tool to applications in vivo," *Lasers in Medical Science* **16**(4), pp. 236–252, 2001.
12. M. Sharifzadeh, D. Zhao, P. Bernstein, and W. Gellermann, "Resonance Raman imaging of macular pigment distributions in the human retina," *Journal of the Optical Society of America A* **25**(4), pp. 947–957, 2008.
13. J. Beattie, S. Brockbank, J. McGarvey, and W. Curry, "Raman microscopy of porcine inner retinal layers from the area centralis," *Mol. Vis* **13**, pp. 1106–1113, 2007.
14. C. Patil, N. Bosschaart, M. Keller, T. van Leeuwen, and A. Mahadevan-Jansen, "Combined Raman spectroscopy and optical coherence tomography device for tissue characterization," *Optics Letters* **33**(10), pp. 1135–1137, 2008.
15. T. Vickers, R. Wambles Jr, And C. Mann, "Curve fitting and linearity: Data processing in Raman spectroscopy," *Applied Spectroscopy* **55**(4), pp. 389–393, 2001.